Scattering From Chiral Cylinders of Arbitrary Cross-Sections Above a Ground Plane

AHSAN ALTAF[ID]1, **HASSAN SAJJAD**[ID]1, **(Graduate Student Member, IEEE),**
CENGIZ OZZAIM2, **(Member, IEEE), AND ERCUMENT ARVAS**1, **(Life Fellow, IEEE)**

1Department of Electrical Engineering, Istanbul Medipol University, 34810 Istanbul, Turkey
2Department of Electrical Engineering, Eskisehir Technical University, 26555 Eskisehir, Turkey

Corresponding author: Ahsan Altaf (ahsan.altaf@std.medipol.edu.tr)

ABSTRACT The main purpose of this work is to solve the problem of electromagnetic scattering from a chiral cylinder of arbitrary cross-section above an infinite perfect electric conducting (PEC) plane. Using image theory, this problem is reduced to two chiral cylinders in free-space. Surface equivalence principle is used to obtain three different equivalent problems for this two-cylinder problem. Then, the method of moments is used to solve these equivalent problems numerically. It is known that the image of a chiral body through a ground plane is another chiral body with the same permittivity and permeability but opposite chirality. Using this property, the two-body problem in the moment method may be reduced to a one-body problem with a complicated moment matrix. Computed numerical results include scattered fields and equivalent surface currents on the cylinder.

INDEX TERMS Image of chiral material, scattering from chiral cylinders above a ground plane.

I. INTRODUCTION

The chiral bodies have been studied by many researchers in the last half-century [1]–[12]. Electromagnetic scattering from chiral bodies in free space has also been studied [13]–[16]. The scattering behavior of a target above a PEC plane can be very different than the behavior in free-space [17]–[32]. Because of the presence of a cross-polarized component, the scattered field from a chiral cylinder, even in free-space, is shown to be quite different than the field scattered from a similar dielectric cylinder [13], [14]. It would be then interesting to see the scattering behavior in the presence of a PEC plane, and that is the motivation behind this work. Fig. 1 is a sample of the results computed by the method used here. It clearly shows how different the scattering behavior can be with the presence of a PEC plane. The details of the method used here are explained in the following sections.

It is shown in [33] that the image of a chiral body above a PEC plane is a chiral body with the same permittivity (ϵ) and permeability (μ). However, the real chiral admittance of the image body is negative of the chiral admittance of the original body. The problem of scattering from a three-dimensional chiral body above a PEC plane is solved in [34] by using
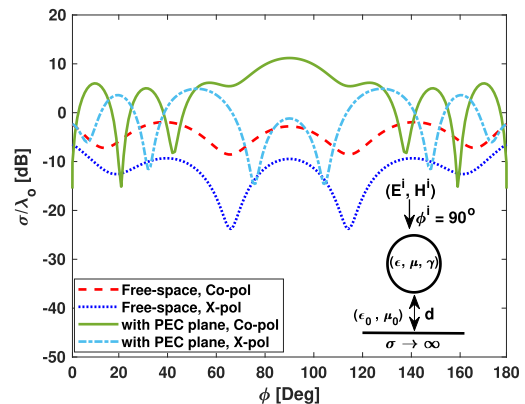
FIGURE 1. Bi-static RCS of a chiral cylinder in free-space and when it is placed above a ground plane, TM excitation, $\phi^i = 90^o$, $\epsilon_r = 4$, $\mu_r = 1$, $\gamma = 0.002$, $r = 0.5\lambda_0$, $d = 0.5\lambda_0$.

image theory and a hybrid FEM-BI procedure. We are not aware of any work solving the problem of electromagnetic scattering from a chiral cylinder of arbitrary cross-section placed above a PEC plane.

The purpose of this work is to solve the problem of electromagnetic scattering from a chiral cylinder of arbitrary cross-section above an infinite PEC plane. This problem is shown in Fig. 2. Here, a chiral cylinder of arbitrary cross-section S_1
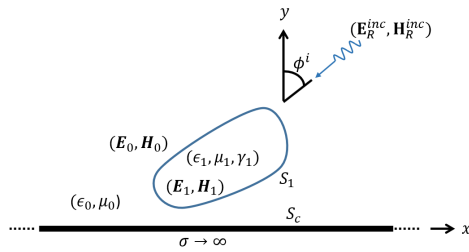
FIGURE 2. The original problem: A chiral cylinder above a ground plane illuminated by a plane wave.

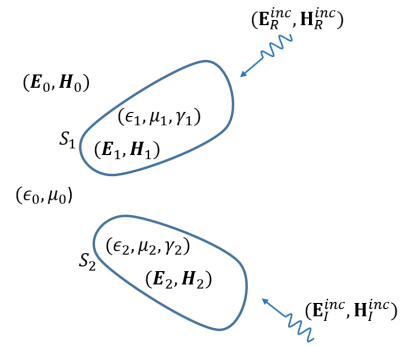**FIGURE 3.** Scattering from two arbitrarily shaped chiral cylinders with different parameters excited by two different incident waves.

is placed above an infinite PEC plane and is illuminated by a known incident plane wave. The purpose is to find the total field at any point above the plane. This problem is solved by first using the image theory to obtain two chiral cylinders in free-space. Then, the surface equivalence principle is used to obtain a set of coupled integral equations for the unknown equivalent surface currents on these two cylinders. Then, the Method of Moments (MoM) is used to solve these integral equations numerically. The moment matrix for this two-cylinder problem is unnecessarily large. The properties of the image body and the image source are used to reduce the size of the moment matrix. This matrix is named as the Enhanced Moment Matrix.

Various different constitutive relations are used for chiral materials [3]–[6]. Here, we use the following,

$$\mathbf{D} = \epsilon \mathbf{E} - j\gamma \mathbf{B} \tag{1}$$

and

$$\mathbf{B} = \mu \mathbf{H} + j\gamma \mu \mathbf{E} \tag{2}$$

where, γ is known as the chiral admittance.

The chiral cylinder in Fig. 2 is characterized by $(\epsilon_1, \mu_1, \gamma_1)$, where ϵ_1 is the permittivity of the body, μ_1 is the permeability, and γ_1 is the chiral admittance. It is placed above a PEC plane at $y = 0$, and is illuminated by an incident plane wave $(\mathbf{E}_R^{inc}, \mathbf{H}_R^{inc})$. The subscript R is used to show that this incident plane wave is due to a real impressed source. This incident wave is either a TM or a TE wave with an angle of incidence ϕ^i. The cylinder is surrounded by free-space (ϵ_0, μ_0). The surfaces of the ground plane and cylinder are denoted by S_c and S_1 respectively. The purpose is to find the total fields $(\mathbf{E}_0, \mathbf{H}_0)$ external to the cylinder, and $(\mathbf{E}_1, \mathbf{H}_1)$ internal to the cylinder.

II. SCATTERING FROM TWO CHIRAL CYLINDERS OF ARBITRARY CROSS-SECTIONS
Consider the problem of electromagnetic scattering from two cylinders illuminated by two different plane waves as shown in Fig. 3. The cylinders may have different cross-sections S_1 and S_2, and different material parameters (ϵ, μ, γ).

It is shown in [33] that the problem of Fig. 3 would be electromagnetically equivalent to the problem in Fig. 2 (for $y \geq 0$), if:

(i) S_2 is the *mirror* image of S_1,
(ii) tangential component of $\mathbf{E}_I^{inc}$ is negative of the tangential component of $\mathbf{E}_R^{inc}$ at $y = 0$,
(iii) $\epsilon_2 = \epsilon_1$, $\mu_2 = \mu_1$, and
(iv) $\gamma_2 = -\gamma_1$.

In this "electromagnetic image problem", the PEC plane of Fig. 2 is replaced by an image cylinder characterized by $(\epsilon_1, \mu_1, -\gamma_1)$ and an image plane wave $(\mathbf{E}_I^{inc}, \mathbf{H}_I^{inc})$. The subscript I is used to show that this incident plane wave is due to an image impressed source.

In this section, we will present the procedure to solve the two-cylinder problem shown in Fig. 3, where the cylinders are assumed to be arbitrary. We will use surface equivalence principle to obtain some coupled integral equations for unknown equivalent surface electric and magnetic currents. We will then solve these integral equations numerically by using MoM. We will also present some results. All computed results are given for the cases where the above three conditions ((i) to (iii)) are satisfied. However, in some cases, γ_2 is assumed to be equal to γ_1, and in some special cases γ_2 is taken to be $-\gamma_1$.

A. INTEGRAL EQUATIONS
Here, surface equivalence principle is used to obtain three equivalent problems for three different regions of Fig. 3.

1) EXTERNAL EQUIVALENCE
Fig. 4 shows an equivalent problem for the problem of Fig. 3 external to the surfaces S_1 and S_2. Here, the whole space is characterized by (ϵ_0, μ_0). The two incident plane waves of Fig. 3 are also kept in Fig. 4. The total fields inside the fictitious surfaces S_1 and S_2 of Fig. 4 are assumed to be zero. The total fields at any point outside these surfaces are assumed to be the same as the total field $(\mathbf{E}_0, \mathbf{H}_0)$ at the same point of Fig. 3. To support the discontinuities of the fields at the surface S_1, equivalent electric and magnetic surface currents $(\mathbf{J}_1, \mathbf{M}_1)$ are placed on this surface. Similarly, equivalent electric and magnetic surface currents $(\mathbf{J}_2, \mathbf{M}_2)$ are placed on the surface S_2. When the fields radiated by these four currents are added to the incident fields in Fig. 4, the result is equal to $(\mathbf{E}_0, \mathbf{H}_0)$ at any point external to S_1 and S_2
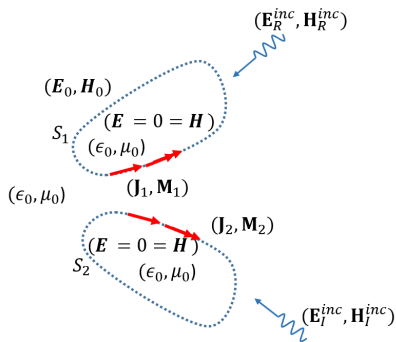
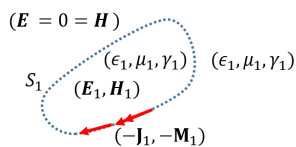**FIGURE 4.** External equivalence for the problem of Fig. 3.

FIGURE 5. Internal equivalence for the real body.

of Fig. 3. However, at any point inside these two surfaces, the sum is equal to zero. In other words,

$$
\mathbf{E}^0_{tan}(\mathbf{J}_1, \mathbf{M}_1) + \mathbf{E}^0_{tan}(\mathbf{J}_2, \mathbf{M}_2)
$$
$$
= -\left[\mathbf{E}^{inc}_R + \mathbf{E}^{inc}_I\right]_{tan} \quad on \quad S_1^- \qquad (3)
$$

and

$$
\mathbf{E}^0_{tan}(\mathbf{J}_1, \mathbf{M}_1) + \mathbf{E}^0_{tan}(\mathbf{J}_2, \mathbf{M}_2)
$$
$$
= -\left[\mathbf{E}^{inc}_R + \mathbf{E}^{inc}_I\right]_{tan} \quad on \quad S_2^- \qquad (4)
$$

Here, the subscript *tan* denotes the tangential component and the superscript "0" denotes that surface currents are radiating in an unbounded external medium (ϵ_0, μ_0). S_1^- and S_2^- refer to the surface just inside S_1 and S_2, respectively. Obviously, similar equations apply for the tangential components of the magnetic field.

2) INTERNAL EQUIVALENCE FOR THE UPPER BODY
Fig. 5 shows an equivalent problem for the problem of Fig. 3 internal to the surface S_1. Here, the whole space is characterized by ($\epsilon_1, \mu_1, \gamma_1$). The two incident plane waves of Fig. 3 are absent here in Fig. 5. The total fields outside the fictitious surface S_1 of Fig. 5 are assumed to be zero. The total fields at any point inside S_1 are assumed to be the same as the total field ($\mathbf{E}_1, \mathbf{H}_1$) at the same point of Fig. 3. To support the discontinuities of the fields at the surface S_1, equivalent electric and magnetic surface currents ($-\mathbf{J}_1, -\mathbf{M}_1$) are placed on this surface. The fields radiated by these two currents (in the unbounded medium ($\epsilon_1, \mu_1, \gamma_1$)) are the same as ($\mathbf{E}_1, \mathbf{H}_1$) at any point inside S_1 of Fig. 3. However, at any point outside S_1, the fields radiated by these currents are zero. In other words,

$$
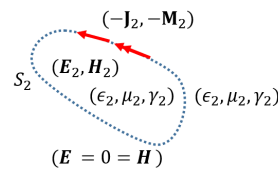\mathbf{E}^1_{tan}(\mathbf{J}_1, \mathbf{M}_1) = 0 \quad on \quad S_1^+ \qquad (5)
$$

where, the superscript "1" denotes that surface currents are radiating in an unbounded medium characterized by ($\epsilon_1, \mu_1, \gamma_1$), and S_1^+ refers to the surface just outside S_1. Obviously, a similar equation applies for the tangential components of the magnetic field.

3) INTERNAL EQUIVALENCE FOR THE LOWER BODY
Fig. 6 shows an equivalent problem for the problem of Fig. 3 internal to the surface S_2. Here, the whole space is characterized by ($\epsilon_2, \mu_2, \gamma_2$). The two incident plane waves of Fig. 3 are absent here in Fig. 6. The total fields outside the fictitious surface S_2 of Fig. 6 are assumed to be zero. The total fields at any point inside S_2 are assumed to be the same as the total field ($\mathbf{E}_2, \mathbf{H}_2$) at the same point of Fig. 3. To support the discontinuities of the fields at the surface S_2, equivalent electric and magnetic surface currents ($-\mathbf{J}_2, -\mathbf{M}_2$) are placed on this surface. The fields radiated by these two currents are the same as ($\mathbf{E}_2, \mathbf{H}_2$) at any point inside S_2. However, at any point outside S_2, the fields radiated by these currents are zero. In other words,

$$
\mathbf{E}^2_{tan}(\mathbf{J}_2, \mathbf{M}_2) = 0 \quad on \quad S_2^+ \qquad (6)
$$

where, the superscript "2" denotes that surface currents are radiating in an unbounded medium characterized by ($\epsilon_2, \mu_2, \gamma_2$), and S_2^+ refers to the surface just outside S_2. Obviously, a similar equation applies for the tangential components of the magnetic field.

B. APPLICATION OF THE MOMENT METHOD
Equations (3) to (6) represent four coupled integral equations for the four unknown currents ($\mathbf{J}_1, \mathbf{M}_1, \mathbf{J}_2, \mathbf{M}_2$). These equations are called EFIE (Electric Field Integral Equations). They are solved here numerically by using the method of moments. First, the cross-sections S_1 and S_2 are each approximated by N linear segments. On each segment there are four unknown currents: the $z-$ and lateral component of the electric current, and $z-$ and lateral component of the magnetic current. Pulses are used as expansion functions for these unknown currents and an approximate Galerkin's method is used for testing. The details are given in [35], [36]. The resulting moment equation is shown in (7), at the bottom of the next page.

The $8N \times 8N$ matrix on the left-hand side of (7) is known as the Moment Matrix. Each element of this moment matrix is an $N \times N$ sub-matrix. The first letter in the name of the sub-matrices in (7) denotes the component of the field. The second letter denotes the source of the field, while the

FIGURE 6. Internal equivalence for the image body.

subscript of the second letter denotes the component of the source current. The third number (1 or 2) represents the surface of the body where the field is computed. The fourth number (1 or 2) represents the surface of the body where the source current resides. Finally, the last number denotes the unbounded medium (0, 1, or 2) in which the source radiates.

For instance, an element in the mth row and the nth column of the sub-matrix ZJ$_Z$110 is the z-component of the electric field on the m^{th} segment of S_1, produced by J$_Z$ on the nth segment of S_1, when this J$_Z$ radiates in the unbounded medium (ϵ_0, μ_0). This element is given by,

$$\text{ZJ}_Z110(m,n) = \frac{-\eta_0 k_0 l_{m_1}}{4} \int_{C_{n_1}} H_0^{(2)}(k_0|\boldsymbol{\rho}_{cm_1} - \boldsymbol{\rho}'|)dl' \quad (8)$$

Here, η_0 and k_0 denote the wave impedance and the wave number of free-space respectively. C_{n_1} represents the nth segment on S_1, and l_{m_1} represents the length of the mth field segment on S_1. The position vector $\boldsymbol{\rho}'$ represents an arbitrary point on C_{n_1} and the position vector $\boldsymbol{\rho}_{cm}$ represents the center of the field segment C_{m_1} on S_1, and $H_0^{(2)}$ is the zeroth order Hankel function of the second kind.

To compute the mn^{th} element of ZJ$_Z$120(m,n), we replace C_{n_1} in (8) with C_{n_2}. Similarly, when we replace in (8), $l_{m_1}, C_{n_1}, \boldsymbol{\rho}_{cm_1}$ with $l_{m_2}, C_{n_2}, \boldsymbol{\rho}_{cm_2}$ respectively, we obtain ZJ$_Z$220(m,n). The elements of ZJ$_Z$210 contain the fields on S_2 produced by the sources on S_1.

The sub-matrices ZJ$_L$110, ZM$_Z$110, ZJ$_L$120, ZM$_Z$120, ZJ$_L$210, ZM$_Z$210, ZJ$_L$220, and ZM$_Z$220 are identically zero.

The sub-matrices in the 2nd row of (7) contain the lateral field on S_1, produced by different sources radiating in the unbounded medium (ϵ_0, μ_0). Therefore, LJ$_Z$110, LM$_L$110, LJ$_Z$120, and LM$_L$120 are identically zero. Similarly, the sub-matrices LJ$_Z$210, LM$_L$210, LJ$_Z$220, and LM$_L$220 are identically zero.

An element in the mth row and the nth column of the sub-matrix ZM$_L$110 is the z-component of the electric field on the m^{th} segment of S_1, produced by M$_L$ on the nth segment of S_1, when this M$_L$ radiates in the unbounded medium (ϵ_0, μ_0). This element is given by,

$$\text{ZM}_L110(m,n) = -j\frac{k_0 l_{m_1}}{4} \int_{C_{n_1}} \hat{n}_1 \cdot \frac{(\boldsymbol{\rho}_{cm_1} - \boldsymbol{\rho}')}{|\boldsymbol{\rho}_{cm_1} - \boldsymbol{\rho}'|}$$
$$\times H_1^{(2)}(k_0|\boldsymbol{\rho}_{cm_1} - \boldsymbol{\rho}'|)dl' \quad (9)$$

Here, $\hat{n}_1 = \hat{t}_{n_1} \times \hat{z}$ is the unit vector normal to the source segment C_{n_1} on S_1, and $\hat{t}_{n_1}$ is the unit vector tangent to the

same segment, and $H_1^{(2)}$ is the first order Hankel function of the second kind. The typical elements of the sub-matrices ZM$_L$120, ZM$_L$210, and ZM$_L$220 have similar form as (9).

An element in the mth row and the nth column of the sub-matrix LJ$_L$110 is the lateral component of the electric field on the m^{th} segment of S_1, produced by J$_L$ on the nth segment of S_1, when this J$_L$ radiates in the unbounded medium (ϵ_0, μ_0).

The $8N \times 1$ column matrix on the left-hand side of (7) contains the unknown expansion coefficients. The $N \times 1$ sub-matrices a and e contain the expansion coefficients for J$_Z$ on S_1 and S_2, respectively. Similarly, b and f contain the expansion coefficients for J$_L$, and c and g contain the expansion coefficients for M$_Z$, and finally, d and h contain the expansion coefficients for M$_L$.

The mth element of $N \times 1$ sub-matrix $-$Zinc1 on the right-hand side of (7) is equal to the negative of the z-component of the total incident electric field on the mth segment of S_1. Similarly, the sub-matrix $-$Zinc2 contains the negative of the z-component of the total incident electric field on S_2. The mth element of the sub-matrices $-$Linc1 and $-$Linc2 represent the lateral component of the total incident electric field on the mth segment of S_1 and S_2 respectively.

Two internal equivalent problems shown in Fig. 5 and Fig. 6 are represented by the last four rows of the moment matrix in (7).

An element in the mth row and the nth column of the sub-matrix ZJ$_Z$111 is the z-component of the electric field on the m^{th} segment of S_1, produced by J$_Z$ on the nth segment of S_1, when this J$_Z$ radiates in the unbounded medium $(\epsilon_1, \mu_1, \gamma_1)$. This element is given by,

$$\text{ZJ}_Z111(m,n) = -\frac{\eta_{c_1} l_{m_1}}{8}\left\{h_1 \int_{C_{n_1}} H_0^{(2)}(h_1|\boldsymbol{\rho}_{cm_1} - \boldsymbol{\rho}'|)dl'\right.$$
$$\left. + h_2 \int_{C_{n_1}} H_0^{(2)}(h_2|\boldsymbol{\rho}_{cm_1} - \boldsymbol{\rho}'|)dl'\right\} \quad (10)$$

where, η_{c_1} is the wave impedance associated with the chiral medium $(\epsilon_1, \mu_1, \gamma_1)$ and is given by the following,

$$\eta_{c_1} = \frac{\eta_1}{\sqrt{1 + (\eta_1 \gamma_1)^2}}. \quad (11)$$

Here, $\eta_1 = \sqrt{\frac{\mu_1}{\epsilon_1}}$. The two wave number h_1 and h_2 associated with the chiral material $(\epsilon_1, \mu_1, \gamma_1)$ are given by the following,

$$h_1 = \omega\mu_1\gamma_1 + \sqrt{(k_1)^2 + (\omega\mu_1\gamma_1)^2} \quad (12)$$

$$\begin{bmatrix}
\text{ZJ}_Z110 & \text{ZJ}_L110 & \text{ZM}_Z110 & \text{ZM}_L110 & \text{ZJ}_Z120 & \text{ZJ}_L120 & \text{ZM}_Z120 & \text{ZM}_L120 \\
\text{LJ}_Z110 & \text{LJ}_L110 & \text{LM}_Z110 & \text{LM}_L110 & \text{LJ}_Z120 & \text{LJ}_L120 & \text{LM}_Z120 & \text{LM}_L120 \\
\text{ZJ}_Z210 & \text{ZJ}_L210 & \text{ZM}_Z210 & \text{ZM}_L210 & \text{ZJ}_Z220 & \text{ZJ}_L220 & \text{ZM}_Z220 & \text{ZM}_L220 \\
\text{LJ}_Z210 & \text{LJ}_L210 & \text{LM}_Z210 & \text{LM}_L210 & \text{LJ}_Z220 & \text{LJ}_L220 & \text{LM}_Z220 & \text{LM}_L220 \\
\text{ZJ}_Z111 & \text{ZJ}_L111 & \text{ZM}_Z111 & \text{ZM}_L111 & 0 & 0 & 0 & 0 \\
\text{LJ}_Z111 & \text{LJ}_L111 & \text{LM}_Z111 & \text{LM}_L111 & 0 & 0 & 0 & 0 \\
0 & 0 & 0 & 0 & \text{ZJ}_Z222 & \text{ZJ}_L222 & \text{ZM}_Z222 & \text{ZM}_L222 \\
0 & 0 & 0 & 0 & \text{LJ}_Z222 & \text{LJ}_L222 & \text{LM}_Z222 & \text{LM}_L222
\end{bmatrix}
\begin{bmatrix} a \\ b \\ c \\ d \\ e \\ f \\ g \\ h \end{bmatrix}
=
\begin{bmatrix} -\text{Zinc1} \\ -\text{Linc1} \\ -\text{Zinc2} \\ -\text{Linc2} \\ 0 \\ 0 \\ 0 \\ 0 \end{bmatrix} \quad (7)$$

and

$$h_2 = -\omega\mu_1\gamma_1 + \sqrt{(k_1)^2 + (\omega\mu_1\gamma_1)^2}. \qquad (13)$$

where,

$$k_1 = \omega\sqrt{\epsilon_1\mu_1}. \qquad (14)$$

An element in the mth row and the nth column of the sub-matrix ZJ_L111 is the z-component of the electric field on the mth segment of S_1, produced by J_L on the nth segment of S_1, when this J_L radiates in the unbounded medium $(\epsilon_1, \mu_1, \gamma_1)$.

An element in the mth row and the nth column of the sub-matrix LJ_L111 is the lateral component of the electric field on the mth segment of S_1, produced by J_L on the nth segment of S_1, when this J_L radiates in the unbounded medium $(\epsilon_1, \mu_1, \gamma_1)$.

The elements in the sub-matrices in the last two rows of the moment matrix of (7) contain the fields computed in the unbounded chiral medium $(\epsilon_2, \mu_2, \gamma_2)$, when these fields are radiated by these surface currents $(\mathbf{J}_2, \mathbf{M}_2)$. The expressions for such elements are similar to those in (10) to (14). For example,

$$ZJ_Z222(m, n) = -\frac{\eta_{c_2}l_{m_2}}{8}\left\{h_3\int_{C_{n_2}} H_0^{(2)}(h_3|\boldsymbol{\rho}_{cm_2} - \boldsymbol{\rho}'|)dl' \right.$$
$$\left. + h_4\int_{C_{n_2}} H_0^{(2)}(h_4|\boldsymbol{\rho}_{cm_2} - \boldsymbol{\rho}'|)dl'\right\} \qquad (15)$$

where, η_{c_2} is the wave impedance associated with the chiral medium $(\epsilon_2, \mu_2, \gamma_2)$ and is given by the following,

$$\eta_{c_2} = \frac{\eta_2}{\sqrt{1 + (\eta_2\gamma_2)^2}}. \qquad (16)$$

Here, $\eta_2 = \sqrt{\frac{\mu_2}{\epsilon_2}}$. The two wave number h_3 and h_4 associated with the chiral material $(\epsilon_2, \mu_2, \gamma_2)$ are given by the following,

$$h_3 = \omega\mu_2\gamma_2 + \sqrt{(k_2)^2 + (\omega\mu_2\gamma_2)^2} \qquad (17)$$

and

$$h_4 = -\omega\mu_2\gamma_2 + \sqrt{(k_2)^2 + (\omega\mu_2\gamma_2)^2}. \qquad (18)$$

where,

$$k_2 = \omega\sqrt{\epsilon_2\mu_2}. \qquad (19)$$

The approximations used and the other details related to computation of the above matrix elements are given in [36].

C. NUMERICAL RESULTS OF TWO CHIRAL CYLINDERS

Consider a system of two circular chiral cylinders as shown in Fig. 7. The cylinders could have completely different cross-sections. However, in this section, the cylinder in the lower half-space is deliberately chosen to be the mirror image of the upper cylinder. The radius r of the cylinders is $0.5\lambda_0$, and the distance d from the center of the cylinders to $y = 0$ plane is λ_0, which is assumed to be 1m. Both cylinders have
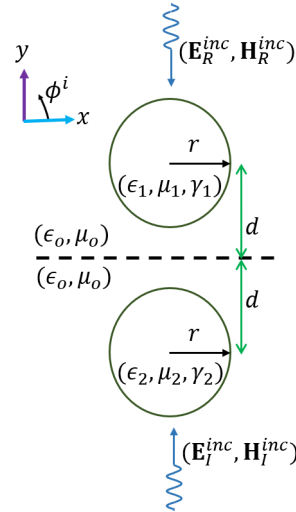
FIGURE 7. Two circular chiral cylinders illuminated by two plane waves.
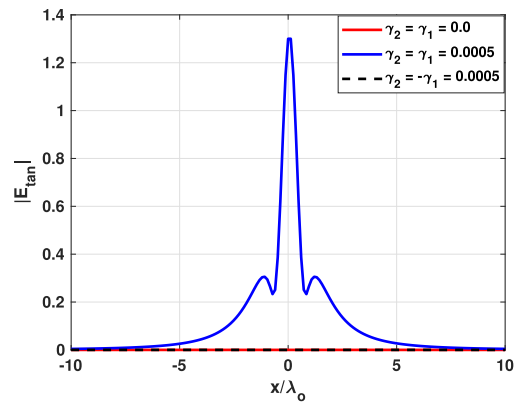
FIGURE 8. Magnitude of the total tangential electric field at $y = 0$ plane of Fig. 7.

$\epsilon_r = 4$, $\mu_r = 1$. Three different values will be assumed for their chiral admittance γ:

(i) $\gamma_1 = \gamma_2 = 0.0$,
(ii) $\gamma_1 = \gamma_2 = 0.0005$, and
(iii) $\gamma_1 = -\gamma_2 = 0.0005$.

The system is illuminated by two TM plane waves. $\mathbf{E}_R^{inc}$ is equal to $\hat{z}1$ (V/m) with incident angle $\phi^i = 90^o$ and $\mathbf{E}_I^{inc}$ is equal to $-\hat{z}1$ (V/m) with incident angle $\phi^i = -90^o$. To use MoM, each cylinder is approximated by $N = 90$ segments.

Using MoM, we first computed the equivalent surface currents (which are not shown here), and then we can find the fields produced by these currents at any point.

Fig. 8 shows the magnitude of the total tangential electric field ($\sqrt{|E_x|^2 + |E_z|^2}$) at $y = 0$ plane of the problem shown in Fig. 7. This field is the sum of the two incident fields and the fields radiated by the equivalent surface currents on both cylinders, when these currents radiate in the unbounded medium (ϵ_0, μ_0), as suggested by Fig. 4.

The red curve in Fig. 8 (for the case $\gamma_1 = \gamma_2 = 0$) shows that the total tangential electric field is zero at $y = 0$ plane.

We also noticed that the currents (not shown here) in the lower cylinder are the images of those on the upper cylinder. These results are expected and agree very well with those presented in [37]. Therefore, it is verified that the image of a dielectric cylinder above a PEC plane is the same dielectric cylinder.

The same results are observed for the dashed black curve in Fig. 8 (for the case $\gamma_1 = -\gamma_2 = 0.0005$), and therefore we can conclude that the image of a chiral cylinder through a PEC plane is another chiral cylinder with real chirality equal to negative of chirality of the original cylinder.

The blue curve in Fig. 8 (for the case $\gamma_1 = \gamma_2 = 0.0005$) shows that the total tangential electric field is not zero at $y = 0$ plane. We also observed that the currents (not shown here) on the lower cylinder are not the image of those on the upper cylinder. Therefore, we can conclude that the image of a chiral cylinder through a PEC plane is not another chiral cylinder with the same parameters.

III. ENHANCED MOMENT MATRIX

As mentioned before, the moment matrix in (7) is unnecessarily large. When correct image theory is used, the equivalent surface currents on the image cylinder are the image of the equivalent currents on the real cylinder. Then, the number of unknowns in (7) would reduce to $4N$ (from $8N$).

To further demonstrate the relationship between the equivalent surface currents on two chiral cylinders, we consider the simple problem shown in Fig. 9. Both cylinders have ($\epsilon_r = 4$, $\mu_r = 1$), and the side lengths (L_x and L_y) are $0.2\lambda_0$. These cylinders are placed at a distance $d = 0.5\lambda_0$ away from the $y = 0$ plane. Here, the cylinders are the mirror image of each other and each is approximated by $N = 3$ segments. (Segment-4 is the image of segment-1, segment-5 is the image of segment-2, and segment-6 is the image of segment-3). The two incident fields are also the image of each other.

The computed results for the surface currents are shown in Table 1 for the case of simple dielectric $\epsilon_r = 4$, $\mu_r = 1$, and $\gamma_1 = \gamma_2 = 0$. In this case, the lower body is the correct image of the upper body. Hence, we expect that the currents on the lower body should be the image of the currents on the upper body. We see from Table 1 that J_Z on an image segment is negative of J_Z on the corresponding original segment. That is, $J_{Z4} = -J_{Z1} = -3.4401 + j0.2069$, $J_{Z5} = -J_{Z2} = 0.7328 + j0.1839$, and $J_{Z6} = -J_{Z3} = -0.5142 + j0.5561$. Therefore, we can see that for the simple dielectric case the expected relationship,

$$e_{n+N} = -a_n, \quad (n = 1, \cdots, N) \tag{20}$$

is satisfied.

Note also that $M_{L4} = M_{L1} = -0.3748 + j0.0208$ in Table 1. According to image theory, the actual M_L current on segment-6 must be negative of the M_L current on segment-3. Since, the arrow on segment-6 is in opposite direction to the arrow on segment-3, we see from Table 1 that $M_{L6} = M_{L3} = -0.6372 - j1.3132$. Similarly, we see that M_{L5} is the image of M_{L2}. Therefore, we can see that for the simple dielectric
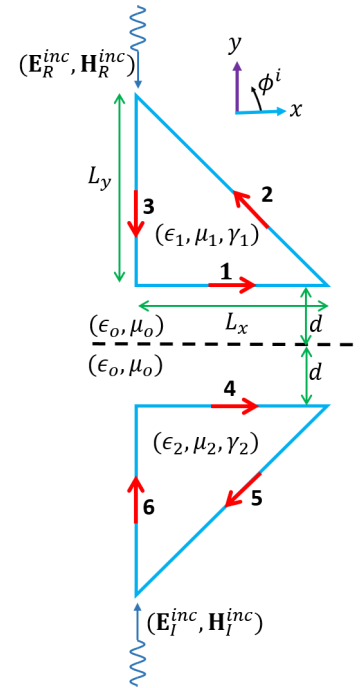

FIGURE 9. Two triangular chiral cylinders illuminated by two plane waves.

case the expected relationship,

$$h_{n+N} = d_n, \quad (n = 1, \cdots, N) \tag{21}$$

is satisfied.

The computed results for the surface currents are shown in Table 2 for the case of two chiral cylinders with $\epsilon_r = 4$, $\mu_r = 1$, and $\gamma_1 = -\gamma_2 = 0.0005$. In this case, the lower chiral body is the correct image of the upper chiral body. Therefore, the equivalent currents on the lower body must be the image of the currents on the upper body. This is correctly shown in Table 2. Therefore, for the correct image problem, in addition to (20) and (21) the following equations are satisfied.

$$f_{n+N} = -b_n, \quad (n = 1, \cdots, N) \tag{22}$$

and

$$g_{n+N} = c_n, \quad (n = 1, \cdots, N). \tag{23}$$

The computed results for the surface currents are shown in Table 3 for the case of two identical chiral cylinders with $\epsilon_r = 4$, $\mu_r = 1$, and $\gamma_1 = \gamma_2 = 0.0005$. Without going into the details, we see that (22) and (23) are not satisfied in this case. Hence, we can quickly conclude that the lower body with $\gamma_1 = \gamma_2$ cannot be the correct image of the original body.

Let us go back to Fig. 3. Let us assume that it represents the correct image problem. That is, S_2 is the mirror image of S_1, the parameters of S_2 are equal to ($\epsilon_1, \mu_1, -\gamma_1$), and the incident field ($\mathbf{E}_I^{inc}, \mathbf{H}_I^{inc}$) is the image field of the original field ($\mathbf{E}_R^{inc}, \mathbf{H}_R^{inc}$). Then, from the preceding discussions, it was concluded that the equivalent surface currents on S_2 are the image of currents on S_1. Then, knowing $a_n, n = 1, \ldots, N$,

TABLE 1. TM excitation, Dielectric Case.

Currents	$\gamma_2 = \gamma_1 = 0$					
	Seg-1 (S_1)	Seg-4 (S_2)	Seg-2 (S_1)	Seg-5 (S_2)	Seg-3 (S_1)	Seg-6 (S_2)
J_Z	3.4401 - j0.2069	-3.4401 + j0.2069	-0.7328 - j0.1839	0.7328 + j0.1839	0.5142 - j0.5561	-0.5142 + j0.5561
J_L	0	0	0	0	0	0
M_Z	0	0	0	0	0	0
M_L	-0.3748 + j0.0208	-0.3748 + j0.0208	-0.5655 - j1.3531	-0.5655 - j1.3531	-0.6372 - j1.3132	-0.6372 - j1.3132

TABLE 2. TM excitation, Chiral Case (Opposite Chiral Admittance).

Currents	$\gamma_2 = -\gamma_1$					
	Seg-1 (S_1)	Seg-4 (S_2)	Seg-2 (S_1)	Seg-5 (S_2)	Seg-3 (S_1)	Seg-6 (S_2)
J_Z	3.2520 - j0.2121	-3.2520 + j0.2121	-0.8314 - j0.1334	0.8314 + j0.1334	0.3985 - j0.4583	-0.3985 + j0.4583
J_L	0.1305 + j0.1165	-0.1305 - j0.1165	-0.0490 + j0.0580	0.0490 - j0.0580	0.0554 + j0.0599	-0.0554 - j0.0599
M_Z	0.0861 + j0.0139	0.0861 + j0.0139	0.0040 + j0.0919	0.0040 + j0.0919	0.0643 + j0.0799	0.0643 + j0.0799
M_L	-0.3235 + j0.0827	-0.3235 + j0.0827	-0.4409 - j1.3418	-0.4409 - j1.3418	-0.5091 - j1.3083	-0.5091 - j1.3083

TABLE 3. TM excitation, Chiral Case (Same Chiral Admittance).

Currents	$\gamma_2 = \gamma_1$					
	Seg-1 (S_1)	Seg-4 (S_2)	Seg-2 (S_1)	Seg-5 (S_2)	Seg-3 (S_1)	Seg-6 (S_2)
J_Z	3.3523 - j0.1889	-3.3523 + j0.1889	-0.7711 - j0.1465	0.7711 + j0.1465	0.4771 - j0.4932	-0.4771 + j0.4932
J_L	-0.0863 - j0.1103	-0.0863 - j0.1103	0.0707 + j0.0506	0.0707 + j0.0506	0.0733 + j0.1874	0.0733 + j0.1874
M_Z	-0.0333 - j0.0031	0.0333 + j0.0031	0.0709 + j0.0410	-0.0709 - j0.0410	0.1133 + j0.0516	-0.1133 - j0.0516
M_L	-0.3448 + j0.0461	-0.3448 + j0.0461	-0.5062 - j1.3663	-0.5062 - j1.3663	-0.5765 - j1.3319	-0.5765 - j1.3319

one knows $e_n, n = N+1, \ldots, 2N$. Similarly, knowing b_n, one knows f_n, and knowing c_n, one knows g_n, and finally knowing d_n, one knows h_n. With these in mind, we can reduce the eight equations in (7) to four equations as follows.

Remembering that some of the sub-matrices in (7) are identically zero, then by adding the 1st row to the 5th row, we get,

$$\left\{ZJ_Z110 - ZJ_Z120 + ZJ_Z111\right\}a_n + \left\{ZJ_L111\right\}b_n$$
$$+ \left\{ZM_Z111\right\}c_n + \left\{ZM_L110 + ZM_L120 + ZM_L111\right\}d_n$$
$$= -Zinc1 \qquad (24)$$

Similarly, adding the 2nd row to the 6th row, we get,

$$\left\{LJ_Z111\right\}a_n + \left\{LJ_L110 - LJ_L120 + LJ_L111\right\}b_n$$
$$+ \left\{LM_Z110 + LM_Z120 + LM_Z111\right\}c_n + \left\{LM_L111\right\}d_n$$
$$= -Linc1 \qquad (25)$$

Adding the 3rd row to the 7th row, we get,

$$\left\{ZJ_Z210 - ZJ_Z220 - ZJ_Z222\right\}a_n + \left\{ZJ_L222\right\}b_n$$
$$+ \left\{ZM_Z222\right\}c_n + \left\{ZM_L210 + ZM_L220 + ZM_L222\right\}d_n$$
$$= -Zinc2 \qquad (26)$$

Finally, adding the 4th row to the 8th row, we get,

$$\left\{LJ_Z222\right\}a_n + \left\{LJ_L210 - LJ_L220 - LJ_L222\right\}b_n$$
$$+ \left\{LM_Z210 + LM_Z220 + LM_Z222\right\}c_n + \left\{LM_L222\right\}d_n$$
$$= -Linc2 \qquad (27)$$

The above four equations, can be written in matrix form as follows.

$$\begin{bmatrix} ZJ_Z1 & ZJ_L1 & ZM_Z1 & ZM_L1 \\ LJ_Z1 & LJ_L1 & LM_Z1 & LM_L1 \\ ZJ_Z2 & ZJ_L2 & ZM_Z2 & ZM_L2 \\ LJ_Z2 & LJ_L2 & LM_Z2 & LM_L2 \end{bmatrix} \begin{bmatrix} a \\ b \\ c \\ d \end{bmatrix} = \begin{bmatrix} -Zinc1 \\ -Linc1 \\ -Zinc2 \\ -Linc2 \end{bmatrix}$$
$$(28)$$

The square matrix in (28) is $4N \times 4N$, and is called the enhanced moment matrix. This matrix is much smaller than $8N \times 8N$ moment matrix in (7). However, the elements of the enhanced matrix are more complicated. For example, the element in the mth row and the nth column of ZJ_Z1 in (28) is equal to the z-component of the electric field produced on segment m^{th} of S_1. This field consists of three parts. The first part is due to J_Z on the nth segment of S_1, when this current radiates in the external medium (ϵ_0, μ_0). The second part is due to the image of this J_Z, when this image current radiates in the external medium (ϵ_0, μ_0). Obviously, this image current is equal to the negative of J_Z, and resides on S_2. The third part is due to J_Z which resides on the mth segment of S_1, when this J_Z radiates in the unbounded medium ($\epsilon_1, \mu_1, \gamma_1$).

The numerical results presented in the following section are computed using the enhanced moment matrix represented by (28).

A. NUMERICAL RESULTS AND DISCUSSIONS

In this section, numerical results for a chiral cylinder of arbitrary cross-section above a PEC plane illuminated by either a TM or a TE plane wave with an angle of incidence (ϕ^i) are presented. The frequency of the incident wave is assumed to be 300 MHz. The results include currents and bi-static radar
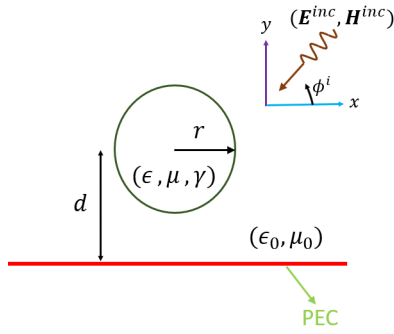
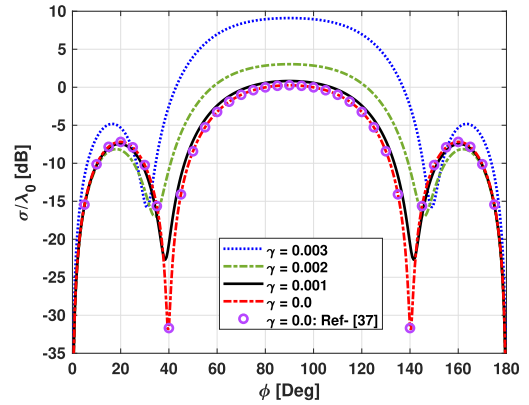**FIGURE 10. A circular chiral cylinder above a PEC plane.**

FIGURE 11. Co-polarized component of the bi-static RCS of a circular chiral cylinder placed above a PEC plane. TM excitation, $\phi^i = 90^o$ for various γ values.

cross section (RCS). First, the expansion coefficients are determined using (28). Then, the scattered fields can easily be computed. The bi-static RCS for $z-$ and $\phi-$ directed scattered fields is defined as,

$$
\begin{aligned}
&\sigma_z(\phi) \\
&= \frac{k_0}{4} \left| \sum_{n=1}^{N} l_{n_1} \left(a_n - \frac{d_n}{\eta_0} \hat{t}_n^1 \cdot \hat{a}_\phi \right) e^{jk_0 \rho^{n_1} \cos(\phi - \phi^{n_1})} \right. \\
&\quad \left. - \sum_{n=N+1}^{2N} l_{n_2} \left(a_n + \frac{d_n}{\eta_0} \hat{t}_n^2 \cdot \hat{a}_\phi \right) e^{jk_0 \rho^{n_2} \cos(\phi - \phi^{n_2})} \right|^2
\end{aligned} \tag{29}
$$

$$
\begin{aligned}
&\sigma_\phi(\phi) \\
&= \frac{k_0}{4} \left| \sum_{n=1}^{N} l_{n_1} \left(\frac{c_n}{\eta_0} + b_n \hat{t}_n^1 \cdot \hat{a}_\phi \right) e^{jk_0 \rho^{n_1} \cos(\phi - \phi^{n_1})} \right. \\
&\quad \left. + \sum_{n=N+1}^{2N} l_{n_2} \left(\frac{c_n}{\eta_0} - b_n \hat{t}_n^2 \cdot \hat{a}_\phi \right) e^{jk_0 \rho^{n_2} \cos(\phi - \phi^{n_2})} \right|^2
\end{aligned} \tag{30}
$$

where, σ denotes the bistatic radar scattering width, l_{n_1} (l_{n_2}) is the length of the nth segment on S_1 (S_2), $\hat{t}_n^1$ ($\hat{t}_n^2$) represents the unit vector tangent to the nth segment (counter-clockwise in the lateral direction) on S_1 (S_2), $\hat{a}_\phi$ is the unit vector in the ϕ-direction at the field point, ρ^{n_1} (ρ^{n_2}) and ϕ^{n_1} (ϕ^{n_2}) are the cylindrical coordinates of the center of the nth segment on S_1 (S_2), η_0 is the free-space wave impedance, and k_0 is the free-space wavenumber.

The results for the problem of scattering from a chiral cylinder above a PEC plane are not available in the literature. Therefore, we used various special cases to validate our computed results. As an example, consider a circular chiral cylinder placed above a PEC plane as shown in Fig. 10. The radius r of the cylinder is $0.1\lambda_0$. The PEC plane is assumed to be at $y = 0$. The distance d between the PEC plane and the center of the cylinder is $0.5\lambda_0$. The cylinder is characterized by $\epsilon_r = 4$, $\mu_r = 1.5$, and a variable chiral admittance γ. It is illuminated by a TM plane wave with $\phi^i = 90^o$. Fig. 11 and 12 show the co- and cross-polarized components of the bi-static scattering width for various values of γ. It is seen from Fig. 11 that as γ reduces to zero, the co-polarized component of the scattering width of the chiral cylinder approaches to that of a regular dielectric cylinder
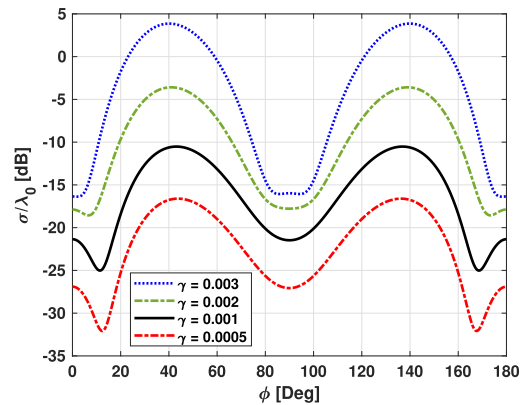

FIGURE 12. Cross-polarized component of the bi-static RCS of a circular chiral cylinder placed above a PEC plane. TM excitation, $\phi^i = 90^o$ for various γ values.
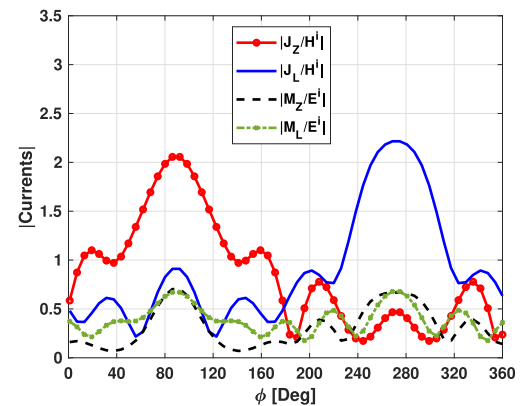

FIGURE 13. Currents on the body for the system shown in Fig. 10, TM excitation, $\phi^i = 90^o$.

of $\epsilon_r = 4$, $\mu_r = 1.5$. The results for the dielectric cylinder above a PEC plane is computed using the approach in [37]. Also, from Fig. 12 we see that as γ approaches zero, the cross-polarized component of the scattering width vanishes. Based on this example, and various other special cases that we considered (and not reported here), we have confidence in our computed results.
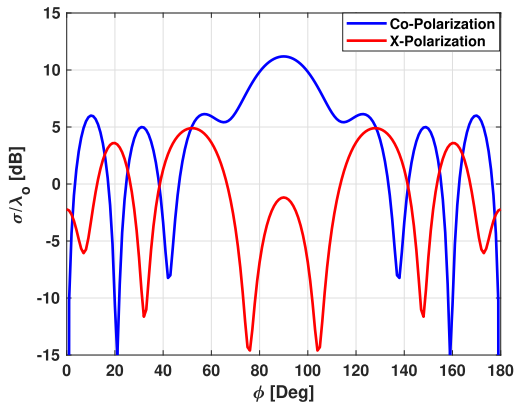
FIGURE 14. Bi-static RCS for the system shown in Fig. 10, TM excitation, $\phi^i = 90^o$.
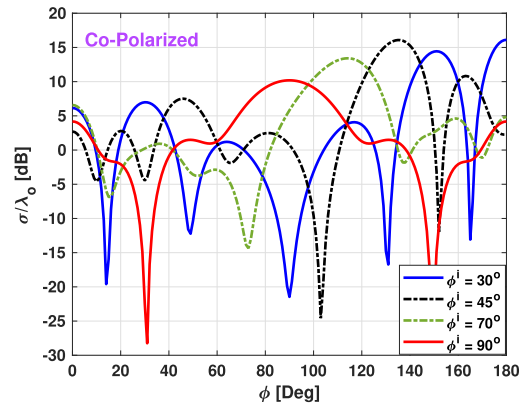

FIGURE 15. Currents on the body for the system shown in Fig. 10, TE excitation, $\phi^i = 90^o$.

FIGURE 16. Bi-static RCS for the system shown in Fig. 10, TE excitation, $\phi^i = 90^o$.

FIGURE 17. Co-polarized component of bi-static RCS for the system shown in Fig. 10, TE excitation for various ϕ^i values.
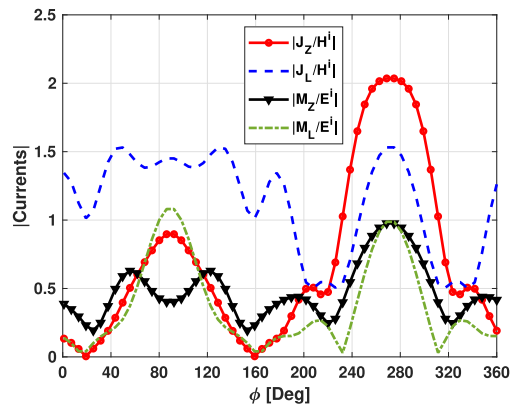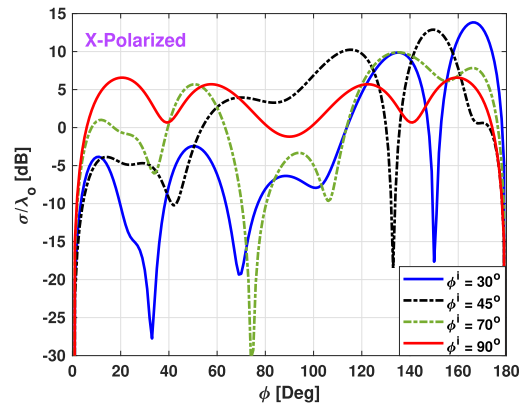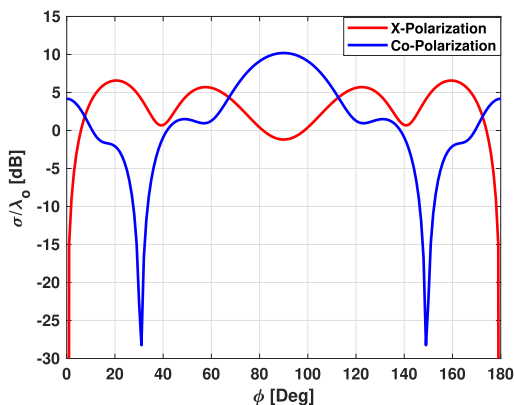

FIGURE 18. Cross-polarized component of bi-static RCS for the system shown in Fig. 10, TE excitation for various ϕ^i values.
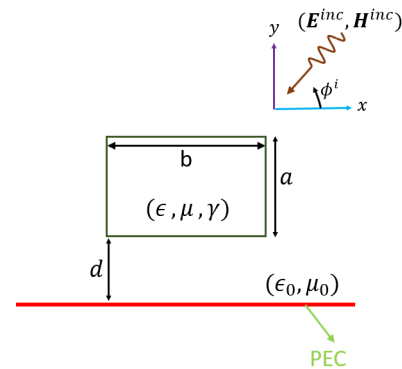

FIGURE 19. A rectangular chiral cylinder above a PEC plane.

Fig. 13 shows the equivalent surface currents on the chiral cylinder of Fig. 10, when $\epsilon_r = 4$, $\mu_r = 1$, $\gamma = 0.002$, and is illuminated by a TM plane wave with $\phi^i = 90^o$. Fig. 14 shows the bi-static RCS for the same setup. Fig. 15 and Fig. 16 show the results when the same cylinder is illuminated by a TE plane wave.

Fig. 17 and Fig. 18 show the bi-static RCS for various different incident angles. Note that, the amplitude of the

co-polarized component has maximum value at the emergence angle as shown in Fig. 17.

Fig. 19 shows a rectangular cylinder of size $0.3\lambda_0 \times 0.15\lambda_0$ above a PEC plane. It is placed at a distance $d = 0.65\lambda_0$ above the PEC plane. The cylinder is characterized by ($\epsilon_r = 4$, $\mu_r = 2$). The chiral admittance γ of the cylinder is varied from 0.0005 to 0.002 with a step of 0.0005. The cylinder is illuminated by a TM plane wave with $\phi^i = 60^o$. The co- and cross-polarized components of bi-static RCS are shown in Fig. 20 and Fig. 21.
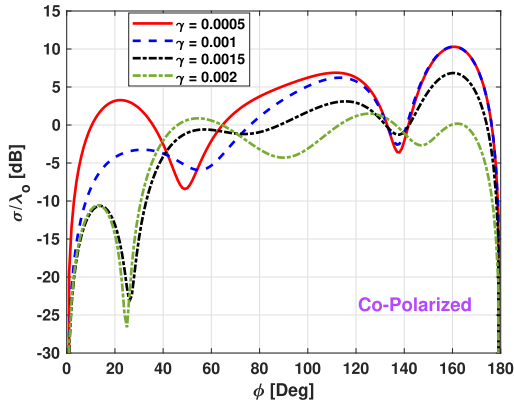
FIGURE 20. Co-polarized component of bi-static RCS for the system shown in Fig. 19, TM excitation, $\phi^i = 60^o$, for various γ values.
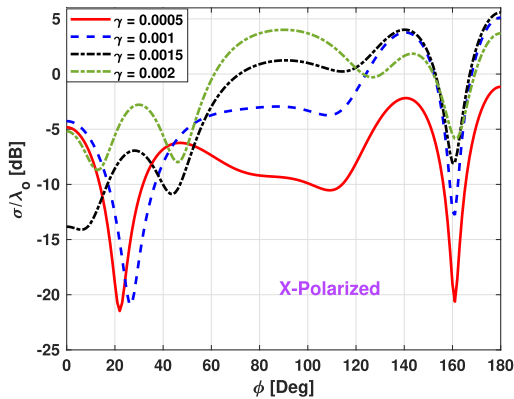

FIGURE 21. Cross-polarized component of bi-static RCS for the system shown in Fig. 19, TM excitation, $\phi^i = 60^o$, for various γ values.
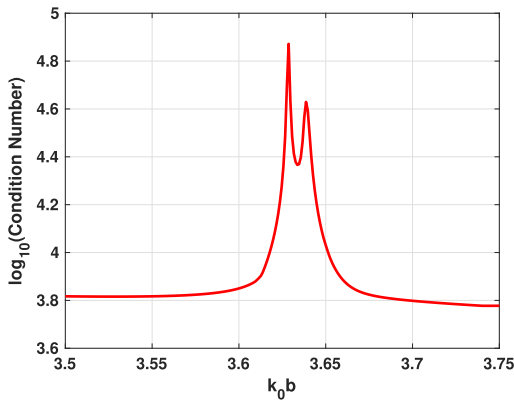

FIGURE 22. Variation of the condition number of the moment matrix with $k_0 b$.

It is known that the EFIE formulation used here fails to give a unique solution when a cylinder is of a spurious "resonant size" [38]. In such cases the moment matrix is highly ill-conditioned and the results computed using such matrices may not be accurate. Therefore, to tell whether the computed results are accurate or not, the condition number of the moment matrix must be monitored.

To demonstrate the behavior of the condition number, consider a rectangular chiral cylinder similar to the one in Fig. 19

with $a = 0.5b$, $d = \lambda_0$, and $\epsilon_r = 4$, $\mu_r = 1$, and $\gamma = 0.0005$. Fig. 22 shows the variation of the condition number of the moment matrix with $k_0 b$. Note that, when $k_0 b = 3.63$ or $k_0 b = 3.64$, the moment matrix is highly ill-conditioned. Therefore, the result obtained under these conditions using EFIE formulation given here may not be accurate. For the cases considered above no abnormality was observed in the value of the condition number. Therefore, we are confident that these results are accurate.

IV. CONCLUSION

A simple moment solution is presented to compute the electromagnetic fields scattered from a chiral cylinder of arbitrary cross-section above a PEC plane. The image theory is used to replace the PEC plane by an image chiral cylinder and an image source. Then, the method of moments is used to formulate the solution to this two-body problem. It was shown that when the image body is legitimate, the two-body problem can be reduced to a one-body problem with a more complicated moment matrix. The condition number of this moment matrix was monitored to ensure the accuracy of the computed results. It was also observed that the computed results for the $\gamma = 0$ case were in excellent agreement with the results obtained by other researchers for the case of a simple dielectric cylinder.

REFERENCES

[1] C. Caloz and A. Sihvola, "Electromagnetic chirality," 2019, *arXiv:1903.09087*. [Online]. Available: http://arxiv.org/abs/1903.09087

[2] C. Caloz and A. Sihvola, "Electromagnetic chirality, Part 2: The macroscopic perspective [electromagnetic perspectives]," *IEEE Antennas Propag. Mag.*, vol. 62, no. 2, pp. 82–98, Apr. 2020.

[3] I. Tinoco and M. P. Freeman, "The optical activity of oriented copper Helices. I. experimental," *J. Phys. Chem.*, vol. 61, no. 9, pp. 1196–1200, Sep. 1957.

[4] D. L. Jaggard, A. R. Mickelson, and C. H. Papas, "On electromagnetic waves in chiral media," *Appl. Phys.*, vol. 18, pp. 211–216, 1979.

[5] E. J. Post, *Formal Structure of Electromagnetics*. Amsterdam, The Netherlands: North-Holland, 1962.

[6] V. K. Varadan, A. Lakhtakia, and V. V. Varadan, "Scattering by beaded helices: Anisotropy and chirality," *J. Wave-Mater. Interact.*, vol. 2, pp. 153–160, 1987.

[7] D. L. Jaggard and N. Engheta, "Chirosorb–as an invisible medium," *Electron. Lett.*, vol. 25, no. 3, p. 173, 1989.

[8] S. Bassiri, C. H. Papas, and N. Engheta, "Electromagnetic wave propagation through a dielectric–chiral interface and through a chiral slab: Errata," *J. Opt. Soc. Amer. A, Opt. Image Sci.*, vol. 7, no. 11, p. 2154, Nov. 1990.

[9] D. L. Jaggard and X. Sun, "Theory of chiral multilayers," *J. Opt. Soc. Amer. A, Opt. Image Sci.*, vol. 9, no. 5, p. 804, May 1992.

[10] A. Lakhtakia, V. V. Varadan, and V. K. Varadan, "What happens to plane waves at the planar interfaces of mirror-conjugated chiral media," *J. Opt. Soc. Amer. A, Opt. Image Sci.*, vol. 6, no. 1, p. 23, Jan. 1989.

[11] I. V. Lindell, A. H. Sihvola, S. A. Tretyakov, and A. J. Viitanen, *Electromagnetic Waves in Chiral and Bi-Isotropic Media*. Norwood, MA, USA: Artech House, 1994.

[12] I. V. Lindell, "Image theory for electromagnetic sources in chiral medium above the soft and hard boundary," *IEEE Trans. Antennas Propag.*, vol. 49, no. 7, pp. 1065–1068, Jul. 2001.

[13] M. A. Al-Kanhal and E. Arvas, "Electromagnetic scattering from a chiral cylinder of arbitrary cross section," *IEEE Trans. Antennas Propag.*, vol. 44, no. 7, pp. 1041–1048, Jul. 1996.

[14] M. S. Kluskens and E. H. Newman, "Scattering by a chiral cylinder of arbitrary cross section," *IEEE Trans. Antennas Propag.*, vol. 38, no. 9, pp. 1448–1455, Sep. 1990.

[15] M. S. Kluskens and E. H. Newman, "Scattering by a multilayer chiral cylinder," *IEEE Trans. Antennas Propag.*, vol. 39, no. 1, pp. 91–96, Jan. 1991.

[16] D. Worasawate, J. R. Mautz, and E. Arvas, "Electromagnetic scattering from an arbitrarily shaped three-dimensional homogeneous chiral body," *IEEE Trans. Antennas Propag.*, vol. 51, no. 5, pp. 1077–1084, May 2003.

[17] A. Kizilay and E. J. Rothwell, "Transient te scattering from a cylinder above an infinite periodic surface using a decomposition method," *J. Electromagn. Waves Appl.*, vol. 15, no. 3, pp. 293–314, Jan. 2001.

[18] R. Rojas, "Integral equations for the scattering by a three dimensional inhomogeneous chiral body," *J. Electromagn. Waves Appl.*, vol. 6, pp. 733–750, Jan. 1992.

[19] I. V. Lindell, A. H. Sihlova, K. O. Muinonen, and P. W. Barber, "Scattering by a small object close to an interface. I. Exact-image theory formulation," *J. Opt. Soc. Amer. A, Opt. Image Sci.*, vol. 8, pp. 472–476, Mar. 1991.

[20] P. J. Valle, F. González, and F. Moreno, "Electromagnetic wave scattering from conducting cylindrical structures on flat substrates: Study by means of the extinction theorem," *Appl. Opt.*, vol. 33, no. 3, p. 512, 1994.

[21] A. Madrazo and M. Nieto-Vesperinas, "Scattering of electromagnetic waves from a cylinder in front of a conducting plane," *J. Opt. Soc. Amer. A, Opt. Image Sci.*, vol. 12, no. 6, pp. 1298–1309, 1995.

[22] P. G. Cottis and J. D. Kanellopoulos, "Scattering from a conducting cylinder above a lossy medium," *Int. J. Electron.*, vol. 65, no. 5, pp. 1031–1038, Nov. 1988.

[23] M. A. Taublatt, "Light scattering from cylindrical structures on surfaces," *Opt. Lett.*, vol. 15, no. 5, pp. 255–257, 1990.

[24] B. Alavikia and O. M. Ramahi, "Electromagnetic scattering from cylindrical objects above a conductive surface using a hybrid finite-element–surface integral equation method," *J. Opt. Soc. Amer. A, Opt. Image Sci.*, vol. 28, no. 12, pp. 2510–2518, 2011.

[25] J. C. Chao, F. J. Rizzo, I. Elshafiey, Y. J. Liu, L. Upda, and P. A. Martin, "General formulation for light scattering by a dielectric body near a perfectly conducting surface," *J. Opt. Soc. Amer. A, Opt. Image Sci.*, vol. 13, no. 2, pp. 338–344, 1996.

[26] S.-C. Lee, "Scattering at oblique incidence by multiple cylinders in front of a surface," *J. Quant. Spectrosc. Radiat. Transf.*, vol. 182, pp. 119–127, Oct. 2016.

[27] R. Lee and A. C. Cangellaris, "Scattering from an arbitrary cylinder in the presence of a parallel planar media interface using the by moment method," *Pier*, no. 4, pp. 345–372, Apr. 991.

[28] P. B. Wong, G. L. Tyler, J. E. Baron, E. M. Gurrola, and R. A. Simpson, "A three-wave FDTD approach to surface scattering with applications to remote sensing of geophysical surfaces," *IEEE Trans. Antennas Propag.*, vol. 44, no. 4, pp. 504–514, Apr. 1996.

[29] R. Borghi, F. Frezza, G. Schettini, F. Gori, and M. Santarsiero, "Plane-wave scattering by a perfectly conducting circular cylinder near a plane surface: Cylindrical-wave approach," *J. Opt. Soc. Amer. A, Opt. Image Sci.*, vol. 13, no. 3, p. 483, 1996.

[30] G. Videen and D. Ngo, "Light scattering from a cylinder near a plane interface: Theory and comparison with experimental data," *J. Opt. Soc. Amer. A, Opt. Image Sci.*, vol. 14, no. 1, pp. 70–78, 1997.

[31] C. Ozzaim, "Plane wave scattering by a conducting cylinder located near an interface between two dielectric half-spaces: A perturbation method," *IEEE Trans. Antennas Propag.*, vol. 65, no. 5, pp. 2754–2758, May 2017.

[32] C. Ozzaim, "A MoM solution for TM scattering by dielectric cylinders above an infinite flat surface," *J. Modern Opt.*, vol. 66, no. 15, pp. 1550–1557, Sep. 2019.

[33] M. S. Kluskens and E. H. Newman, "Image theory for chiral bodies," *IEEE Trans. Antennas Propag.*, vol. 39, no. 5, pp. 676–677, May 1991.

[34] Y.-J. Zhang and E.-P. Li, "Scattering of three-dimensional chiral objects above a perfect conducting plane by hybrid finite element method," *J. Electromagn. Waves Appl.*, vol. 19, no. 11, pp. 1535–1546, Jan. 2005.

[35] M. A. Alkanhal, "Electromagnetic scattering from chiral cylinders of arbitrary cross section," Ph.D. dissertation, Dept. Elect. Eng. Comput. Sci., Syracuse Univ. Syracuse, NY, USA, 1994.

[36] A. Altaf, "Scattering from a chiral cylinder of arbitrary cross-section above a ground plane," Ph.D. dissertation, Dept. Elect. Electron. Eng., Istanbul Medipol Univ., Istanbul, Turkey, 2020.

[37] E. Arvas, S. M. Rao, and T. K. Sarkar, "E-field solution of TM-scattering from multiple perfectly conducting and lossy dielectric cylinders of arbitrary cross-section," *IEE Proc. H Microw., Antennas Propag.*, vol. 133, no. 2, p. 115, 1986.

[38] E. Arvas and J. R. Mautz, "On the non-uniqueness of the surface EFIE applied to multiple conducting and/or dielectric bodies," *AEU. Archiv Elektronik Ubertragungstechnik*, vol. 42, no. 6, pp. 364–369, 1988.

AHSAN ALTAF received the B.Sc. degree (Hons.) in electronics engineering from COMSATS University, Pakistan, in 2012. He is currently pursuing the Ph.D. degree in electrical engineering with Istanbul Medipol University, Turkey. From 2012 to 2015, he was a Laboratory Engineer with the Department of Electrical Engineering, City University, Pakistan. His research interests include MIMO antenna system, RF/Microwave devices, scattering of electromagnetic waves, and computational electromagnetics. He was a recipient of the Gold Medal from the COMSATS University.

HASSAN SAJJAD (Graduate Student Member, IEEE) received the B.S. degree in telecommunication engineering from FAST-NUCES, Pakistan, in 2009, and the M.S. degree in electrical engineering from Linnaeus University, Vaxjo, Sweden, in 2012. He is currently pursuing the Ph.D. degree in electrical engineering with Istanbul Medipol University, Turkey. From 2012 to 2014, he was a Researcher with the Department of Electrical Engineering, King Saud University, Riyadh, Saudi Arabia. His research interests include electromagnetic scattering problems, RF/microwave devices, antenna design, and mutual coupling compensation in antenna arrays.

CENGIZ OZZAIM (Member, IEEE) received the B.S.E.E. and M.S.E.E. degrees from Middle East Technical University, Ankara, Turkey, in 1987 and 1991, respectively, and the Ph.D. degree from Clemson University, Clemson, SC, in 1999. From 1994 to 1999, he was a Research Assistant with Clemson University. He is currently a Professor with the Department of Electrical Engineering, Eskisehir Technical University, Eskisehir, Turkey. His current research interests are dielectric resonator antennas and scattering of electromagnetic waves in chiral medium.

ERCUMENT ARVAS (Life Fellow, IEEE) was born in Van, Turkey, in 1953. He received the B.Sc. and M.Sc. degrees in electrical engineering from Middle East Technical University, Ankara, Turkey, in 1976 and 1979, respectively, and the Ph.D. degree in electrical engineering from Syracuse University, Syracuse, NY, USA, in 1983. From 1983 to 1984, he was with the Department of Electrical Engineering, Yildiz Technical University, Istanbul, Turkey. From 1984 to 1987, he was with the Rochester Institute of Technology, Rochester, NY, USA, and from 1987 to 2014, he was with Syracuse University. He is currently with the Department of Electrical and Electronics Engineering, Istanbul Medipol University, Istanbul, Turkey. His research interests include electromagnetics scattering and microwave devices. He is a Life Fellow of the Electromagnetics Academy.

● ● ●